



ELSEVIER

Available online at [www.sciencedirect.com](http://www.sciencedirect.com)

ScienceDirect

journal homepage: [www.elsevier.com/locate/hydro](http://www.elsevier.com/locate/hydro)

# Neutron radiography analysis of a hydride-based hydrogen storage system

A. Baruj<sup>a,b,c,\*</sup>, E.M. Borzone<sup>a,b</sup>, M. Ardito<sup>b</sup>, J. Marín<sup>a</sup>, S. Rivas<sup>a</sup>,  
F. Roldán<sup>a</sup>, F.A. Sánchez<sup>a,b</sup>, G. Meyer<sup>a,b,c</sup>

<sup>a</sup> Centro Atómico Bariloche, CNEA, 8400 Bariloche, Argentina

<sup>b</sup> Instituto Balseiro, CNEA-U.N. Cuyo, 8400 Bariloche, Argentina

<sup>c</sup> CONICET, Argentina

## ARTICLE INFO

### Article history:

Received 2 December 2014

Received in revised form

26 June 2015

Accepted 28 June 2015

Available online 21 July 2015

### Keywords:

Neutrography

Neutron imaging

AB5

In-situ experiment

## ABSTRACT

A hydrogen container based on the use of a hydride forming material (LaNi<sub>5</sub>) has been specifically designed for performing in-situ Neutron Imaging experiments. The device allows following the process of heat-induced hydrogen release from the initially fully hydrided material. A reaction front forms in the material around the central heater. As the experiment proceeds, the front expands radially. Later on, heat conduction by the container walls produces the decomposition of the hydride in contact with them. As a consequence, and for the implemented geometry, the front advances at an almost constant radial speed. A simple analysis of the images contrast allows the quantification of the ratio between the hydride and metal phases for the complete experiment.

Copyright © 2015, Hydrogen Energy Publications, LLC. Published by Elsevier Ltd. All rights reserved.

## Introduction

Neutron Imaging (NI) comprises a series of techniques that transform the interaction between neutrons and an object under study into optical images. Among them, neutron radiography (or *neutrography*) is a transmission visualization technique based on the interaction of neutrons with the elements of a material [1]. It is somehow comparable to X-rays radiography. However, while X-rays interactions depend monotonically on the atomic number of the elements, neutron interaction with matter is related to a cross section

that varies not only from element to element but even between different isotopes of an element. In particular, light elements that are virtually invisible to X-rays, like hydrogen or boron, produce strong interactions with neutrons [2]. Conversely, there are heavier elements that produce strong X-rays contrast, like aluminum or zirconium, which are weak neutron attenuators [2]. In addition, neutron penetration of materials is considerably higher than that of X-rays. These characteristics turn neutron radiography (NR) into a useful visualization technique for situations involving strong neutron attenuators such as water, polymers or other hydrogen compounds [3–7].

\* Corresponding author. Centro Atómico Bariloche, CNEA, 8400 Bariloche, Argentina.

E-mail address: [baruj@cab.cnea.gov.ar](mailto:baruj@cab.cnea.gov.ar) (A. Baruj).

<http://dx.doi.org/10.1016/j.ijhydene.2015.06.146>

0360-3199/Copyright © 2015, Hydrogen Energy Publications, LLC. Published by Elsevier Ltd. All rights reserved.

The NR technique can be applied to the study of hydride forming materials (HFM) for hydrogen storage, as demonstrated early on by Sakaguchi et al. [8,9]. They used NR to detect hydrogen in Mg<sub>2</sub>Ni storage alloys, following the first stages of hydride formation and quantifying the amount of hydrogen in the material. Later on, Jacobson et al. [4] and Wood et al. [10] used a combination of NI techniques to study the reaction pattern of an AB<sub>5</sub> alloy inside a cylindrical container during hydrogen absorption. Their results show that the formation of the hydride phase inside the container is not homogeneous but strongly depends on the material localization. Pranzas and collaborators performed in-situ studies of hydrogen sorption in a massive reactor containing NaAlH<sub>4</sub>/TiF<sub>3</sub> powder [11,12]. Their results show how the powder, evenly distributed inside the container at the beginning of the experiments, is affected by the hydrogen inflow. The striking images display the formation of a tree-like structure after the first hydrogenation cycle which essentially remains after the following cycles of hydrogen charge/discharge. The non-even powder distribution can negatively affect the container overall performance as a hydrogen storage system.

A particularly interesting example of NI applied to the study of HFM is the work of Gondek et al. [13] which presents a step-by-step observation of the hydride formation process in an AB<sub>5</sub> alloy inside a container. The images show that hydriding occurs first near the container walls, thanks to the higher heat conduction of Al in comparison to the powder.

The processes of hydrogen incorporation and release by a massive hydride-based storage container are usually not observable due to the metallic container walls. However, it has been established that they are largely dominated by the poor thermal conductivity of the hydride forming material [14]. When considering containers design, a great deal of attention is placed on improving heat exchange between the powder material and external heat source/sink. NR may provide useful information about how hydriding and dehydriding reactions take place inside a container. This information could serve to elaborate functional container models, aiding container design for improved heat exchange and reaction kinetics. Considering the NR technique potential, the amount of publications related to hydrogen storage studies is relatively small. One of the reasons is that these studies usually involve managing relatively large amounts of hydrogen at high pressure which could be considered dangerous at NR facilities nearby experimental nuclear reactors or other neutron sources. Another reason is that hydride-based storage containers are usually built with thick steel walls that affect NR contrast, although there are examples of Al made containers [11–13]. Our approach consisted in designing a steel/aluminum container suitable for following hydride reactions by means of NR without losing the usual characteristics of massive hydride-based hydrogen storage devices, i.e. containing a relatively large amount of HFM and keeping the possibility of conducting pressure and temperature triggered processes.

This work is then aimed at using NR as a tool for in-situ following reactions inside a massive hydride-based hydrogen storage container. In particular, we present the container design, describe the specific experimental setup and

discuss the results corresponding to the case of thermally induced hydrogen release from the fully hydrided material.

## Experimental

### Neutron radiography facility

For this work, we have used the NR facility of RA-6 experimental nuclear reactor at Centro Atomico Bariloche, Argentina. The facility provides a 20 cm × 20 cm square neutron beam. By design, the ratio between the source to sample longitude (L) and beam aperture (D) is fixed to 100 (L/D = 100). With the reactor operating at 500 kW, the neutron fluxes are 2.54 × 10<sup>6</sup> n/cm<sup>2</sup>s (thermal) and 2.93 × 10<sup>4</sup> n/cm<sup>2</sup>s (epithermal). The detection system collects the transmitted beam and consists of a 20 cm × 20 cm scintillation screen made of 6LiF/ZnS doped with Ag, made by Applied Scintillation Technologies. The scintillation screen light peak is at λ = 450 nm. The light is reflected out of the beam path by a set of two front surface mirrors in order to protect the CCD camera from the incoming radiation. A Schneider Kreuznach Xenon condensing lens focuses the image onto the camera. Both, the lens and the camera are placed inside a light-tight box. The camera is a Penguin 600 CLM from Pixera Corporation. It has a maximum resolution of 2776 pixels × 2074 pixels and provides digital depth of 16 bits. The CCD dark current is reduced by a four stage thermoelectric Peltier cooling device.

In NR experiments, the neutron transmittance (T) of a material is usually calculated from the ratio between the transmitted (I) and incident (I<sub>0</sub>) intensities as [15]:

$$T = \frac{I}{I_0} = \exp(-\sigma \rho d/M) \quad (1)$$

where σ is the total neutron cross section of the material, d is its thickness, ρ the material density (in g/cm<sup>3</sup>) and M the atomic weight (in g/mol). This expression does not take into account the possibility of having multiple scattering effects and it is the simplest description of the experiment.

### Hydride-based hydrogen storage device

The container is a cylinder with a stainless steel body and two aluminum lids for mechanical resistance. A detailed description of the container design can be found in Ref. [16]. Here, we only present its main characteristics. The body has been machined from a 304L stainless steel single piece (Fig. 1a). Stainless steel was selected because it does not react with most HFM and has poor thermal conductivity and good temperature resistance in comparison to other metals (e.g. aluminum). The cylinder is 14 mm high and has external and internal diameters of 125 mm and 88 mm, respectively. The cylinder floor is 1 mm thick. The floor has a central hole where a small Cu cylinder that hosts a resistive heater was placed and welded. The body cavity is filled with the HFM (LaNi<sub>5</sub>) and closed by an upper 304L stainless steel lid with a thickness of 3.2 mm that rests over an O-ring. The cavity height and stainless steel floor and lid thicknesses were chosen by considering their impact on the contrast of NR images, a task aided by computer calculation with a home-made program

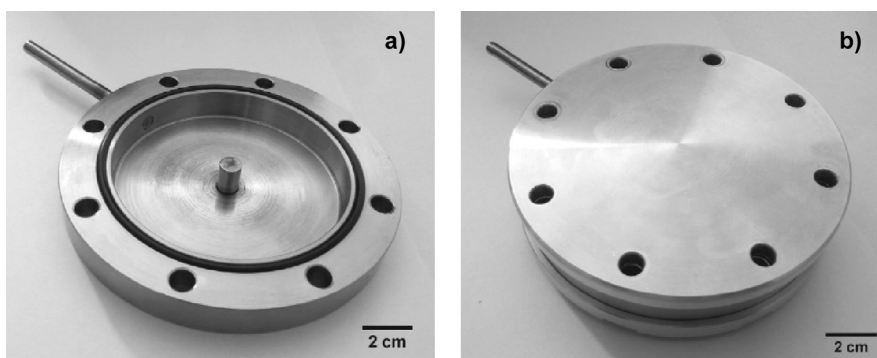


**Fig. 1** – a) Stainless steel body of the HFM container. The central cylinder hosts a 100 W resistive heater. The tube on the upper left corner is the hydrogen inlet/outlet. b) Container shown with the front and rear aluminum lids in position.

based on Eq. (1) and the neutron beam characteristics of the facility. In addition, the ASME Section VIII code and a mechanical finite element model of the device were used to analyze its mechanical resistance. The results showed that the thickness of stainless steel floor and lid was not enough to withstand the required pressure range. In order to reach the required mechanical resistance without compromising NR contrast, a couple of aluminum lids were added each of them with a diameter of 130 mm and 6.8 mm thickness (Fig. 1b). A 1/4" stainless steel tube was inserted in the cavity side and welded to its inner wall to serve as hydrogen inlet/outlet. A 0.5  $\mu\text{m}$  sintered stainless steel filter and a ball valve were attached to this tube. Finally, a 100 W cartridge resistive heater was placed inside the central Cu cylinder with a PT-100 resistance temperature detector (RTD) attached to it for temperature control. Upon construction, the empty container was subjected to a 30 bar hydraulic test and, afterwards, its tightness tested with hydrogen at 20 bar. Then, it was cleaned and filled with 200 g of  $\text{LaNi}_5$  slumps (purity 99.9%, REacton) inside an Ar glove box. The HFM was activated inside the container by applying several pressure cycles between 0 bar and 10 bar.

### Experimental setup

Fig. 2 is a schematic view of the experimental setup used at the RA-6 NR facility. The idea for this experiment is to start with the HFM completely hydrided, to produce hydrogen release by providing heat with the central heater and to investigate whether a dehydriding front forms in the material. In order to avoid pressure build up, the released hydrogen is stored in a 50 l gas cylinder which has an initial pressure slightly above the equilibrium pressure of  $\text{LaNi}_5$  at room temperature (2.5 bar).

The HFM container was placed in the NR chamber with the front lid facing the incident neutron beam. The container valve (V-A) was connected with a Cu tube and a high pressure hose to the gas cylinder via a gas feed through (FT), a ball valve (V-C) and a one-way valve. This one-way valve was placed to ensure that hydrogen only flows from the HFM container into the gas cylinder. A manometer (P) allows reading the pressure in the gas circuit during the experiment. A vacuum pump is connected to the gas circuit via a ball valve (V-B) in order to evacuate the air from the system before the experiment starts.

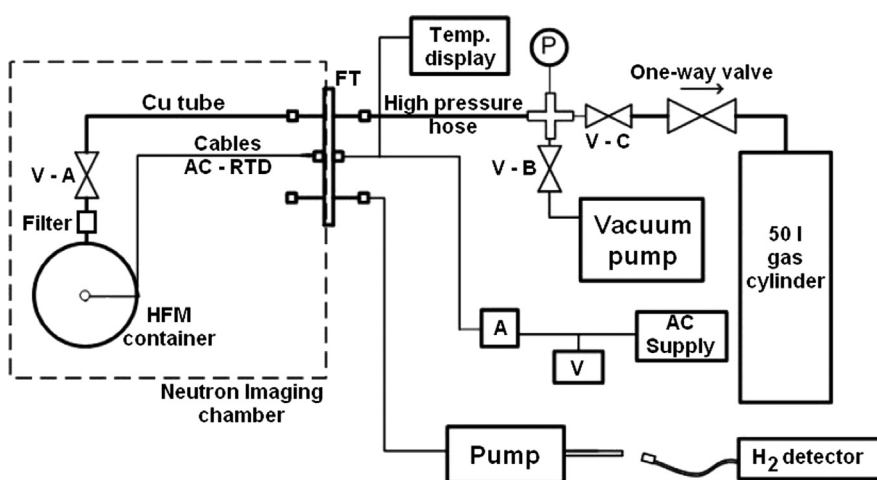


**Fig. 2** – Schematic drawing of the experimental setup at the NI facility of the RA-6 experimental nuclear reactor. Details are provided in the main text.

An AC supply provides electrical power to the central 100 W heater. During the experiment, it was controlled manually with a variable transformer (Variac). Temperature readings from the resistance temperature detector (RTD) attached to the heater were displayed next to the pressure meter. Both readings were available to the experiment research team and to the reactor operator. For security reasons, experiment cutoff values for both readings were established ( $T_{\text{heater}} = 500\text{ }^{\circ}\text{C}$ ,  $P = 5\text{ bar}$ ). Additionally, a gas pump continuously extracted air from the NI chamber. A  $\text{H}_2$  detector (sniffer type) was placed next to the pump exhaust. The experiment would be immediately terminated upon  $\text{H}_2$  detection there.

Additionally, a setup similar to that of Fig. 2 but including a volumetric device [17] was used under laboratory conditions. The volumetric device uses a flow controller to dynamically measure hydrogen release from the material. This previous experiment allowed to find out the relevant operation parameters and to test the in-situ experiment beforehand.

The in-situ experiment procedure was as follows. The HFM container was filled with hydrogen until the material was completely hydrided. Hydrogen in gaseous phase was kept at 2.5 bar, that is the equilibrium pressure of  $\text{LaNi}_5$  at room temperature. In this condition, and with valve V–A closed, the HFM container was taken to the NR facility and attached to the experimental setup shown in Fig. 2. Then, the following steps were performed:

- i) Evacuation: The gas connections (Cu tube and high pressure hose) were evacuated by starting up the vacuum pump and opening valve V–B. After this step, V–B was closed.
- ii) The gas pump and  $\text{H}_2$  detector were started.
- iii) Valves V–A and V–C were opened.
- iv) The beam line was opened and the reactor power increased to 500 kW. The monitoring of pressure and temperature cutoff values, and  $\text{H}_2$  presence started.
- v) First images were taken. The selected exposure time was 40 s (at ISO: 50). The resolution was set at  $1392 \times 1040$  pixels, 16 bit depth.
- vi) The AC power supply was started and the experiment began. The heater power was set at 50 W and its temperature was  $(355 \pm 10)\text{ }^{\circ}\text{C}$  during the experiment.
- vii) Images were taken for 67 min. For the sake of clarity, we identify the pictures by an index going from p0 (beginning of the experiment) to p48 (end of the experiment).
- viii) Experiment finish: The AC power supply was turned off. Valves V–A and V–C were closed. The system was evacuated using the vacuum pump. The neutron beam shutter was closed and the reactor power decreased.
- ix) Images for background (i.e., without the container) and dark field (i.e., with the neutron shutter closed) corrections were taken under operation conditions similar to those used during the experiment.

### Image processing

NR images were saved during the experiment with the TIFF format. Afterwards, they were processed and analyzed using

the ImageJ software, version 1.46r [18]. The dark field file was subtracted from every image (including the background file). Afterwards, every experiment image was divided by the corrected background. A median filter with a mask radius of 1 pixel was applied to remove bad pixels. The resulting images were rotated and cropped to the area of interest. No further modifications were applied to the images. Fig. 3a and b show an example of a representative image before and after processing. In order to relate the transmittance to the ratio between hydrided and dehydrided material, an annular mask was applied selecting the inner area of the HFM container as shown in Fig. 3c, in order to eliminate the heater and central Cu insert.

## Results

### NR pictures

Fig. 4 shows NR pictures representative of the complete heat-induced dehydriding process. Fig. 4a corresponds to the initial state.  $\text{LaNi}_5$  is completely hydrided ( $\text{LaNi}_5\text{H}_6$ ) and it is seen with a dark contrast due to its hydrogen content. The tube on the right hand side is the hydrogen inlet/outlet and the wire (seen with a darker contrast in the image) corresponds to the resistive heater and RTD electrical connections. The heater is placed at the center of the HFM container. The zone with a clearer contrast at the top of the HFM container corresponds to an empty volume (void), left on purpose in order to allow the material expansion during the hydriding process.

After the power supply is turned on, the heater temperature elevates. About 10 min later, the advance of a dehydriding front proceeding from the center is observed (Fig. 4b–e). An area with a clearer contrast appears around the central heater due to the hydrogen release from that portion of the material. Later, as the process proceeds, the contrast of the surrounding area, still hydrided, also becomes clearer (Fig. 4d and e). This effect is a consequence of the heat transmitted by the metal structure of the HFM container which dehydrides the material in contact with the walls. This is in agreement to what was observed by Gondek et al. [13] for the hydriding process: heat transport by the metal walls accelerates the reaction of the material in contact with them. Another visible effect is the contraction experimented by the material as the dehydriding process advances. This contraction is due to the volume difference between the hydrided and non-hydrided materials which is over 20%. As a consequence of this volume difference, radial cracks appear in the HFM (Fig. 4d–f). In addition, the material separates from the cylinder walls. Fig. 4f corresponds to a state where  $\text{LaNi}_5$  is completely dehydrided. A sequence containing all acquired images has been included as Supplementary Content in a digital video format archive.

Supplementary data related to this article can be found online at <http://dx.doi.org/10.1016/j.ijhydene.2015.06.146>.

### Images analyses

Integrated radial profile graphs were obtained by applying a polar transform to the masked images (Fig. 3c). The areas

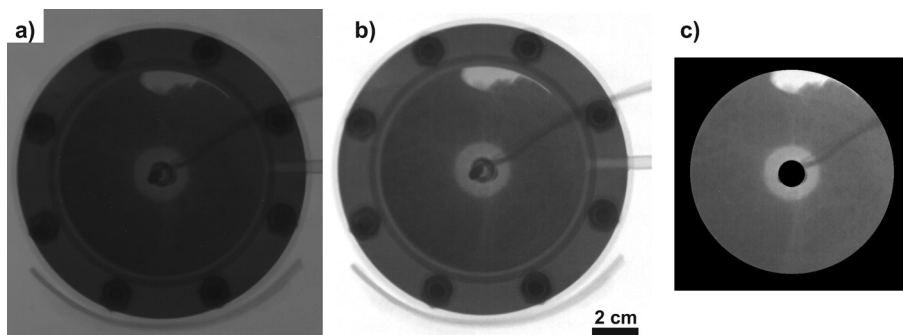


Fig. 3 – Example of the applied image processing. a) Original image. b) Processed Image. c) Analyzed area.

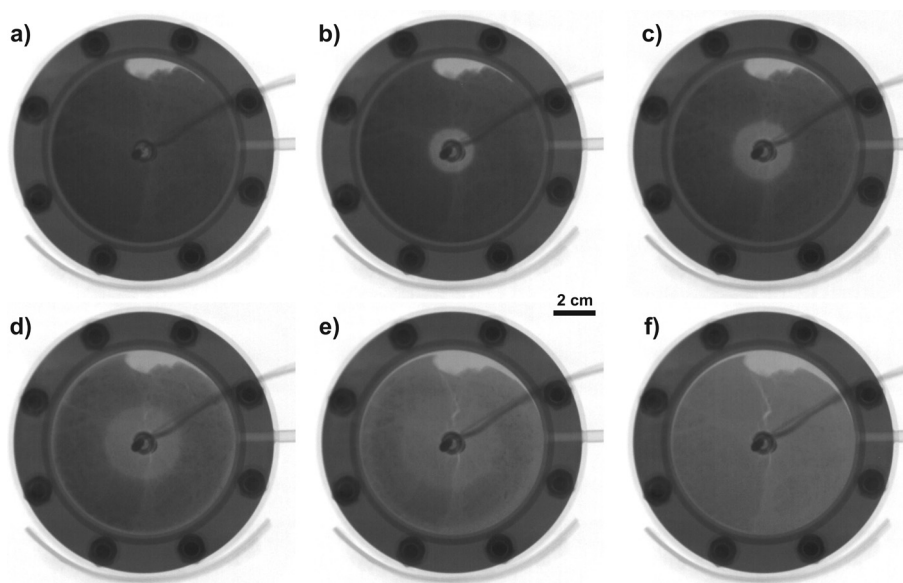


Fig. 4 – Selected images of the experiment sequence. a) Picture p0, initial state, b) Picture p12, after 1370 s,  $T_{\text{heater}} = 354\text{ }^{\circ}\text{C}$ , c) Picture p21, after 2002 s,  $T_{\text{heater}} = 361\text{ }^{\circ}\text{C}$ , d) Picture p30, after 2682 s,  $T_{\text{heater}} = 357\text{ }^{\circ}\text{C}$ , e) Picture p39, after 3266 s,  $T_{\text{heater}} = 359\text{ }^{\circ}\text{C}$ , f) Picture p48, after 4026 s, final state. At the early stages of the process a well-defined reaction front forms near the heating element. As the process continues the heat transfer through the HFM container walls becomes important and the hydride decomposes more evenly.

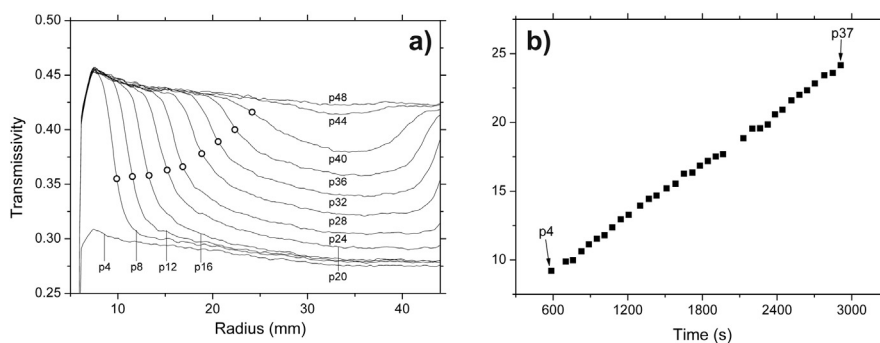


Fig. 5 – (a) Integrated polar profiles for selected images. The empty dot in each profile marks the position of the reaction front (middle of the transmittance step). (b) Position of the reaction front versus time (from profile p4 to p37).

corresponding to the void and the wire seen in the original images have been excluded in the processing. Selected radial intensity profiles are shown in Fig. 5a. The first images present a low transmittance (low gray levels, darker colors) throughout the complete radius of the HFM container. Profiles of pictures p8 to p20 present a well-defined step between a lighter inner ring, corresponding to the metallic dehydrided material, and the darker outer area corresponding to the hydride. This step marks the location of the reaction front, for which a radial position and thickness can be defined. Profiles p24 to p40 also display a step that can be related to the position of the dehydriding reaction front. In addition, the zone to the right of the step has a transmittance that is higher as the profile number progresses and that is always above than that seen in the previous profiles. This occurs because the heat transfer by the container metal walls causes the decomposition of the hydride near them. Then, the material is dehydriding not only due to the heat received from the central heater but it is also receiving enough heat from the container walls to dehydride from the walls into the interior. Profiles p44 and p48 were taken near the completion of the dehydriding process. It is difficult to identify a dehydriding front in these profiles due to the effect mentioned before.

Fig. 5b is a plot of the hydride front position as a function of the experiment elapsed time. The hydride front position has been assigned to the distance from the center of the container to the middle of the transmittance step seen in the corresponding profile. Fig. 5b shows an almost linear dependence between the front position and time. Considering an ideal model of uniform heat transfer from a central heater in a cylindrical geometry, the dehydriding front should move at a slower speed as the time increases [19,20]. In this case, heat transfer from the container walls plays an important role in defining this behavior because when this effect starts to show up (from profile p24) dehydriding proceeds not only from the center of the cylinder but also in the transversal direction. As a result, the dehydriding front advances into an increasingly

thinner hydride region at a constant speed. This is indeed an effect of the selected geometry and heat transfer conditions set by the materials selection that would be very difficult to model a-priori. The result then makes apparent one of the main advantages of the neutron imaging technique: the possibility of studying the real life behavior of hydride-based components, and the chance to obtain useful data for computer simulation models.

### Quantitative analysis

By analyzing masked images, of which Fig. 3c is an example, histograms of neutron transmittance were constructed for each image. Fig. 6 presents the histograms corresponding to the six images shown in Fig. 4. Three distinct peaks are observed in these histograms. The smaller one on the right, with a transmittance around 0.66, corresponds to the void area inside the container, particularly the upper part of the HFM container (Fig. 4). As the experiment proceeds, this peak area increases due to the contraction of the HFM during the dehydriding process. The middle peak, at a transmittance level around 0.45, corresponds to the metal (dehydrided) phase. This middle peak is not present in the first image and reaches its maximum value in the last one. The left hand side peak corresponds to the darker area in the images. In the first image, as the HFM is completely hydrided, the peak corresponds to the hydride phase. As the experiment proceeds, the peak is composed by contributions from both hydride and metallic phases. For this reason, as the reaction advances, the position of this peak shifts from the value corresponding to the hydride to the one corresponding to the metal, and its position is related to the ratio between these phases.

In order to quantify the fraction of material in each phase from the images, the histograms were adjusted by using lognormal peak functions. Gaussian and lorentzian functions did not provide a satisfactory fit to the data. The area of each peak in the histogram is proportional to the number of pixels

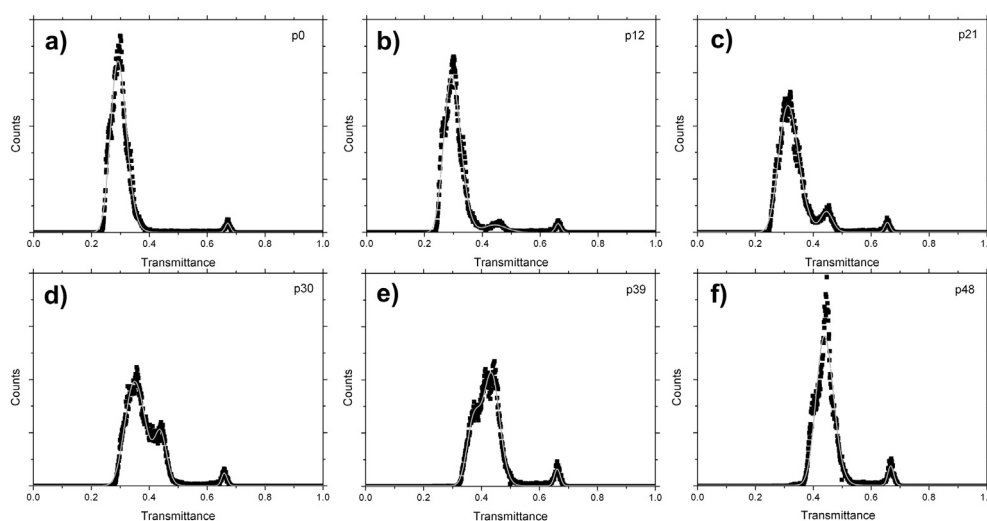


Fig. 6 – Transmittance histograms of the selected images shown in Fig. 4 a) Picture p0 (initial state), b) Picture p12, c) Picture p21, d) Picture p30, e) Picture p39, f) Picture p48 (final state). Fitting functions, composed by three independent lognormal peaks, are included as solid lines for reference.

in the image that present that range of transmittance which, in turn, is proportional to the amount of material in the corresponding state.

As the reaction proceeds, the area of the void peak increases slightly due to the material's volume decrease. At the same time the metal peak grows as the reaction front advances. Finally, the peak corresponding to a combination of hydride and metal phases shrinks and moves towards the position of the metal peak as its metal-to-hydride ratio  $R_{MH}$  increases. To estimate this ratio based on the position of the peak, the following expression was used:

$$R_{MH} = (C_1 - C_H)/(C_M - C_H) \quad (2)$$

There,  $C_M$  is the position of the center of the metal peak,  $C_H$  is the center of the hydride peak and  $C_1$  is the center of the mixed peak. In this way, the total fraction  $F_i$  of the image corresponding to each phase ( $i = M, H, v$  for metal, hydride and void, respectively) is given by

$$F_H = \left[ A_1 \frac{(C_M - C_1)}{(C_M - C_H)} \right] / \sum_i A_i \quad (3)$$

$$F_M = \left[ A_1 \frac{(C_1 - C_H)}{(C_M - C_H)} + A_2 \right] / \sum_i A_i \quad (4)$$

$$F_v = A_3 / \sum_i A_i \quad (5)$$

where  $A_{1,2,3}$  is the area of the corresponding peak. The results are shown in Fig. 7. The time dependence of the amount of hydride material obtained through this method closely resembles the one measured by volumetric techniques during the experiment performed under similar conditions at the laboratory, lending credit to the above estimation.

It should be noted that this analysis was performed without considering multiple scattering effects. The fact that

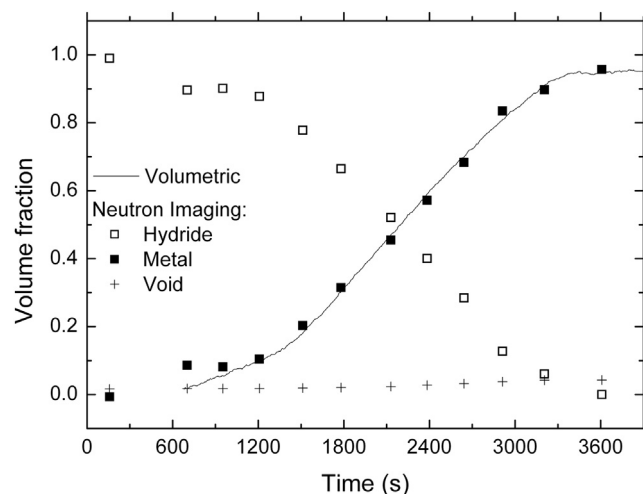


**Fig. 7 – Time dependence of the fraction corresponding to the hydride, the metal and the void area, as estimated from the transmittance histograms. Metal fraction measured by means of a separately volumetric experiment is included for comparison (solid line).**

the results from neutron radiography and volumetric experiments are in good agreement lends support to the applied procedure.

## Conclusions

The HFM container, specifically designed for NR experiments, allowed the in-situ observation of the heat induced hydrogen release process by an initially fully hydrided material ( $\text{LaNi}_5\text{H}_6$ ). A reaction front forms in the HFM around the central heater. As the experiment proceeds, the front expands radially. Later on, heat conduction by the container walls produces the dehydrogenation of the material in contact with them. As a consequence, the front advances at an almost constant radial speed. A simple analysis of the images grey levels allowed the quantification of the ratio between the hydride and metal phases for the complete set of pictures. The results show that NR is a useful technique for designing massive hydrogen containers based on HFM and for understanding their behavior under real working conditions.

## Acknowledgments

The authors gratefully acknowledge G. Facchini and J. Promet for their technical assistance during the experiment setup. This work has been funded by ANPCyT (PAE 36985 and PICT 2012-1796), U.N. Cuyo (Project 06/C417) and by ANPCyT-CNEA through fellowships from PFDT-PRH 200.

## REFERENCES

- [1] Berger H. Advances in neutron radiographic techniques and applications: a method for nondestructive testing. *Appl Radiat Isot* 2004;61:437–42.
- [2] Heller AK, Brenizer JS. Neutron radiography. In: Anderson IS, McGreevy RL, Bilheux HZ, editors. *Neutron imaging and applications: a reference for the imaging community*. NY, USA: Springer; 2009.
- [3] Yasuda R, Matsubayashi M, Nakata M, Harada K. Application of neutron radiography for estimating concentration and distribution of hydrogen in zircaloy cladding tubes. *J Nucl Mater* 2002;302:156–64.
- [4] Jacobson DL, Hussey DS, Baltic E, Udovic TJ, Rush JJ, Bowman Jr RC. Neutron imaging studies of metal-hydride storage beds. *Int J Hydrogen Energy* 2010;35:12837–45.
- [5] Farahmand M, Boston AJ, Grint AN, Nolan PJ, Joyce MJ, Mackin RO, et al. Detection of explosive substances by tomographic inspection using neutron and gamma-ray spectroscopy. *Nucl Instrum Methods Phys Res B* 2007;261:396–400.
- [6] Sedighi-Gilani M, Griffo M, Mannes D, Lehmann E, Carmeliet J, Derome D. Visualization and quantification of liquid water transport in softwood by means of neutron radiography. *Int J Heat Mass Trans* 2012;55:6211–21.
- [7] Selamet OF, Pasaogullari U, Spornjak D, Hussey DS, Jacobson DL, Mat MD. Two-phase flow in a proton exchange membrane electrolyzer visualized in situ by simultaneous neutron radiography and optical imaging. *Int J Hydrogen Energy* 2013;38:5823–35.

- [8] Sakaguchi H, Kohzai A, Hatakeyama K, Fujine S, Yoneda K, Kanda K, et al. Visualization of hydrogen in hydrogen storage alloys using neutron radiography. *Int J Hydrogen Energy* 2000;25:1205–8.
- [9] Sakaguchi H, Satake Y, Hatakeyama K, Fujine S, Yoneda K, Matsubayashi M, et al. A nalysis of hydrogen distribution in hydrogen storage alloy using neutron radiography. *J Alloy Compd* 2003;354:208–15.
- [10] Wood BM, Ham K, Hussey DS, Jacobson DL, Faridani A, Kaestner A, et al. Real-time observation of hydrogen absorption by LaNi<sub>5</sub> with quasi-dynamic neutron tomography. *Nucl Instrum Methods Phys Res B* 2014;324:95–101.
- [11] Pranzas PK, Boesenberg U, Karimi F, Muenning M, Metz O, Bonatto Minella C, et al. Characterization of hydrogen storage materials and systems with photons and neutrons. *Adv Eng Mater* 2011;13:730–6.
- [12] Bellosta von Colbe JM, Metz O, Lozano GA, Pranzas PK, Schmitz HW, Beckmann F, et al. Behavior of scaled-up sodium alanate hydrogen storage tanks during sorption. *Int J Hydrogen Energy* 1012;37:2807–2811
- [13] Gondek Ł, Selvaraj NB, Czub J, Figiel H, Chapelle D, Kardjilov N, Hilger A, et al. Imaging of an operating LaNi<sub>4.8</sub>Al<sub>0.2</sub>-based hydrogen storage container. *Int J Hydrogen Energy* 2011;36:9751–7.
- [14] Wang XL, Suda S. Reaction kinetics of hydrogen-metal hydride systems. *Int J Hydrogen Energy* 1980;15:569–77.
- [15] ASTM Standard E748, 2002(2008). Standard practices for thermal neutron radiography of materials. West Conshohocken, PA: ASTM International; 2003. <http://dx.doi.org/10.1520/E0748-02R08>. [www.astm.org](http://www.astm.org).
- [16] Baruj A, Ardito M, Marín J, Sánchez F, Borzone EM, Meyer G. Design and characterization of a hydride-based hydrogen storage container for neutron imaging studies. *Phys Procedia*, 10th World Conference on Neutron Radiography 2015 [Accepted].
- [17] Meyer G, Rodriguez D, Castro F, Fernández G. Automatic device for precise characterization of hydride-forming materials. In: Veziroğlu TN, Winter CJ, Baselt JP, Kreysa G, editors. *Proc. 11th world hydrogen energy conference2*. Stuttgart: Germany; 1996. p. 1293–8.
- [18] Rasband WS. ImageJ. Bethesda, Maryland, USA: U. S. National Institutes of Health; 1997–2014. <http://imagej.nih.gov/ij/>.
- [19] Incropera FP, DeWitt DP, Bergman TL, Lavine AS. *Fundamentals of heat and mass transfer*. 6th ed. Hoboken, NJ: John Wiley & Sons; 2007.
- [20] Nakaso K, Shigenaga R, Fukai R. Effect of heat transfer enhancement on energy release rate from a metal hydride tank. *J Chem Eng Jpn* 2007;40:1257–63.